

Under the Paperwork Reduction Act of 1995, no persons are required to respond to a collection of information unless it contains a valid OMB control number.

**Certificate of Mailing under 37 CFR 1.8**

I hereby certify that this correspondence is being deposited with the United States Postal Service with sufficient postage as first class mail in an envelope addressed to:

Commissioner for Patents  
P.O. Box 1450  
Alexandria, VA 22313-1450

on 5/25/2005  
Date

  
\_\_\_\_\_  
Signature

Brian Kolbowski  
Typed or printed name of person signing Certificate

36,847  
Registration Number, if applicable

(216) 649-0376  
Telephone Number

Note: Each paper must have its own certificate of mailing, or this certificate must identify each submitted paper.

This collection of information is required by 37 CFR 1.8. The information is required to obtain or retain a benefit by the public which is to file (and by the USPTO to process) an application. Confidentiality is governed by 35 U.S.C. 122 and 37 CFR 1.11 and 1.14. This collection is estimated to take 1.8 minutes to complete, including gathering, preparing, and submitting the completed application form to the USPTO. Time will vary depending upon the individual case. Any comments on the amount of time you require to complete this form and/or suggestions for reducing this burden, should be sent to the Chief Information Officer, U.S. Patent and Trademark Office, U.S. Department of Commerce, P.O. Box 1450, Alexandria, VA 22313-1450. DO NOT SEND FEES OR COMPLETED FORMS TO THIS ADDRESS. **SEND TO: Commissioner for Patents, P.O. Box 1450, Alexandria, VA 22313-1450.**

If you need assistance in completing the form, call 1-800-PTO-9199 and select option 2.

**BEST AVAILABLE COPY**

**IN THE UNITED STATES PATENT AND TRADEMARK OFFICE**

In Re:	Application of Prince et al.	)	
		)	
Serial No.:	10/766,225	)	
		)	Art Unit 3644
Filed:	January 28, 2004	)	
		)	
For:	Aircraft and Missile Forebody	)	
	Flow Control Device and	)	
	Method of Controlling Flow	)	
		)	
Examiner:	Galen L. Barefoot	)	
		)	
Cuyahoga County	)		
	) SS:		
State of Ohio	)		

**AFFIDAVIT OF FREDERICK J. LISY**  
**37 C.F.R. § 1.131 AFFIDAVIT**

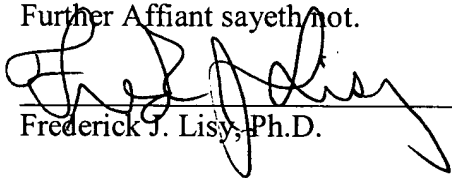
Affiant, Frederick J. Lisy, having been duly sworn according to law, deposes and states as follows:

1. I am one of the inventors and applicants of the invention entitled "Aircraft and Missile Forebody Flow Control Device and Method of Controlling Flow" disclosed and claimed in U.S. Patent Application Serial No. 10/766,225 filed on January 28, 2004.
2. The invention described and claimed in the application was conceived prior to December 20, 2002, as evidenced by the following facts which are of my own knowledge.
2. Attached as Appendix A is a paper, which was given before the American Institute of Aeronautics and Astronautics during their 1<sup>st</sup> AIAA Flow Control Conference from 24-26 of June 2002 in St. Louis, Missouri.
3. The paper in Appendix A describes a missile comprising a forebody with at least one flow effector on the missile forebody and at least one sensor having a signal on the missiles forebody, the at least one sensor being positioned to detect flow separation or side forces on the missile forebody, and a closed loop control system; wherein the closed loop control system is used for activating and deactivating the at least one flow effector

based on at least in part the signal of the at least one sensor. In addition the paper, describes tests that were performed using our entire system including a closed loop control system.

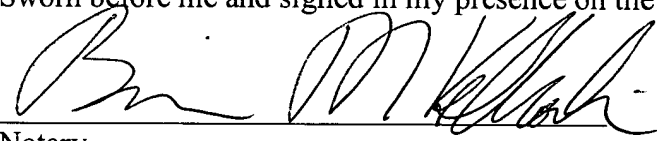
4. Prior to December 20, 2002 we had disseminated all the information related to the conception and actual reduction to practice of our invention to our attorney who worked diligently in preparing our patent application, which he filed on January 3, 2003.

Further Affiant sayeth not.

  
Frederick J. Lisy, Ph.D.

**NOTARY**

Sworn before me and signed in my presence on the 23<sup>rd</sup> day of May, 2005.

  
Notary

**BRIAN M. KOLKOWSKI, ATTORNEY  
NOTARY PUBLIC, STATE OF OHIO  
MY COMMISSION HAS NO EXPIRATION DATE**



AIAA 2002-2827

## **Deployable Flow Effectors for Phantom Yaw Control of Missiles at High Alpha**

**Mehul P. Patel, Troy S. Prince, Reed Carver, Jack M. DiCocco,  
and Frederick J. Lisy**

Orbital Research Inc.  
Cleveland, OH

**T. Terry Ng**

University of Toledo  
Toledo, OH

**1<sup>st</sup> AIAA Flow Control Conference**

**24-26 June 2002, St. Louis, Missouri**

# DEPLOYABLE FLOW EFFECTORS FOR PHANTOM YAW CONTROL OF MISSILES AT HIGH ALPHA

Mehul P. Patel,<sup>\*</sup> Troy S. Prince,<sup>†</sup> Reed Carver,<sup>‡</sup> Jack M. DiCocco,<sup>§</sup> and Frederick J. Lisy<sup>\*\*</sup>

Orbital Research Inc., Cleveland, OH 44143

T. Terry Ng<sup>††</sup>

Dept. of Mechanical, Industrial, and Manufacturing Engineering

The University of Toledo, Toledo, OH 43606

## Abstract

A high alpha phantom yaw control system for enhanced missile maneuverability and stabilization control has been developed. Open and closed-loop experiments on a fin-less 3:1 tangent ogive missile model were conducted to quantify the control effectiveness of the high alpha phantom yaw control system. The flow control system utilizes co-located actuators and sensors modules, force balance data, and a closed-loop controller. The co-located actuators and sensors modules incorporate eight deployable flow effectors and eight corresponding dynamic pressure sensors located circumferentially near the tip of the missile nose cone. Deployable flow effectors are active micro-vortex generators that control and manipulate pressure distribution along the forebody to produce significant side forces and yawing moments for missile control. Significant side forces caused by crossflow separation and natural baseline asymmetries were observed between 40° and 60° alpha. Deployable flow effectors were efficacious between 40° to 55° alpha in generating large side forces that cancelled the baseline flow asymmetry and producing yawing moments on either side of the slender body. Results demonstrate that flow effectors can be used to achieve a wide spectrum of control forces and to modulate the side forces around the missile forebody for desired effect. Dynamic test results showed that the closed-loop controller was successfully able to control the yawing moment on the missile during sweeps from 0° to 60° alpha at various sweep rates. Closed-loop experiments demonstrated the control system's ability to maintain a desired side force corresponding to zero, left and right yaw.

## Nomenclature

$\alpha$	(alpha) angle of attack, deg
$Re_d$	freestream Reynolds number based on model diameter, $\rho U_o d / \mu$
$U_o$	freestream velocity
$\mu$	absolute viscosity
$d$	missile model diameter
$\beta$	angle of sideslip, deg
$\theta$	DFE radial location on nose cone, deg
$C_n$	yawing-moment coefficient, $M_z / q S_{ref} d$
$C_Y$	Side-force coefficient, $F_Y / q S_{ref}$
$M_z$	yawing moment
$F_Y$	side force
$S_{ref}$	cross-sectional area of cylindrical portion of missile model, $\pi d^2 / 4$
$PID$	Proportional Integral Derivative
$K_p$	proportional gain of the PID control law
$K_i$	integral gain of the PID control law
$K_d$	derivative gain of the PID control law

## Introduction

Significant progress has been made in the last two decades towards achieving supermaneuverability of missiles and fighter aircraft at high alpha. A classic example demonstrating the tactical advantage of a supermaneuverable aircraft over other aircraft during a combat situation is the Herbst maneuver by the X-31.<sup>1,2</sup> Next generation high performance missiles face a much greater challenge where mission requirements dictate evasive maneuvers at high alpha.<sup>3</sup>

It has long been recognized that slender bodies of revolution at high alpha encounter separation- and vortex-induced phantom yaw caused by asymmetric

<sup>\*</sup> Senior Aerodynamicist, Member AIAA

<sup>†</sup> Mechanical and Controls Engineer, Member AIAA

<sup>‡</sup> Physicist, Member AIAA

<sup>§</sup> Aerospace Engineer, Member AIAA

<sup>\*\*</sup> Vice President, Member AIAA

<sup>††</sup> Professor, Senior Member AIAA

vortex shedding,<sup>4-6</sup> even at zero angle of sideslip.<sup>7</sup> Large side forces and dynamic out-of-plane loading occur for alpha ranging from 30 to 60 degrees. Researchers have concluded that the out-of-plane loads result from micro-asymmetries on the surface of the nose cone such as small dents, cracks in the paint, and other microscopic imperfections near the tip of the nose cone.<sup>8,9</sup> It has also been shown that these asymmetries are affected by the bluntness of the forebody, Reynolds Number, roll angle, and alpha. At high alpha, these side forces are especially pronounced due to the increasing ineffectiveness of traditional control surfaces. Side forces resulting from these asymmetries adversely affect the missile's overall performance and significantly limit flight envelope. However, proper exploitation of these forces can offset natural side forces and produce desired side forces that substantially increase maneuverability at high alpha by controlling the system of vortices along the forebody.

Demand for high alpha missile control has led to a number of investigations on the subject.<sup>10-14</sup> Research conducted by Herbst,<sup>1</sup> and later followed by Ericsson and Beyers,<sup>15</sup> demonstrated the ability to achieve increased maneuverability on a X-31 aircraft for extreme aerial combat situations using thrust vectoring and advanced control schemes. The success of the X-31 program was in part due to efficient flow control on the forebody of the aircraft. Other investigators have used various forms of geometric changes such as nose bluntness,<sup>16</sup> strakes,<sup>17</sup> boundary layer strips,<sup>18,19</sup> and rotating nose tips<sup>20</sup> to control the asymmetric vortices off the forebody. A single symmetric strake and a splitter-plate-fin were also used to suppress the flow asymmetry.<sup>21,22</sup> It was shown that the splitter-plate-fin did not have to extend far downstream of the apex for controlling the asymmetric loads. Controlled disturbances at the near-apex flow region were able to control the flow downstream due to strong three-dimensional flow effects. Blowing has also been demonstrated to control forebody flow symmetry.<sup>23</sup> Recent accomplishments in micro-blowing have demonstrated that vortex instabilities can be manipulated with small controlled perturbations introduced near the region of maximum flow sensitivity, i.e. nose of the forebody.<sup>24</sup>

Passive flow control techniques, such as transition strips and nose bluntness, are somewhat effective in alleviating aerodynamic loads, but are limited by increased drag and loss of vortex-induced lift on the forebody. This necessitates a need for active flow control methods that; (1) control both the magnitude and direction of side forces, (2) improve missile maneuverability by exploiting asymmetric vortices, and (3) have flow effectors that retract to minimize drag when the system is not needed.

Researchers have investigated various active flow control techniques such as jet blowing,<sup>25</sup> unsteady

bleed<sup>26</sup>, suction<sup>27</sup> and blowing, and Deployable Flow Effectors<sup>28</sup> (DFEs). These techniques typically operate in an open-loop mode with no sensor feedback. Thus, there is a need to develop a closed-loop control system to fully realize the potential of active control actuators for missile-control enhancement. Recently, researchers have demonstrated feasibility of closed-loop control systems for high-alpha maneuvering via numerical<sup>29</sup> and experimental<sup>30</sup> investigations. Bernhardt and Williams<sup>30</sup> demonstrated the ability of the closed-loop control system to control the coning angle of the model, its rotation rate, and the direction of rotation using a pair of suction ports on either side of the nosecone tip. The desired input and the output command in closed-loop control system by Bernhardt and Williams<sup>30</sup> was the pressure coefficient and not the actual yawing moments.

Despite numerous investigations, a closed-loop flow control system to fully realize the potential for enhanced maneuverability of missiles at high alpha has yet to be identified. This paper presents progress towards the development of a high-alpha phantom yaw control system for control of forebody flow asymmetries utilizing dynamic pressure sensors and DFEs coupled with a closed-loop controller. Details of this control system are presented along with results from open and closed-loop control experiments.

### DFEs Based Phantom Yaw Control System

The phantom yaw control system for control of missile forebody flow asymmetries at high alpha relies upon the effectiveness of DFEs in generating on-demand side forces around the missile body for a desired yawing moment. DFEs are active micro-vortex generators that effectively control the pressure distribution along the forebody, yielding large side forces and yawing moments for control of yaw on either side of the forebody. The DFEs are small mechanical tabs made from epoxy glass-fabric with dimensions of 0.9 x 0.3 x 0.08 cm, and are placed underneath the surface of the model in their retracted state (non-obtrusive to the flow). Upon controlled deployment, the DFEs interact with the forebody vortical flowfield to generate a desired yawing moment at high alpha. The presented forebody model utilized eight DFEs located circumferentially around the nose cone of the missile body. Single, or combinations of DFEs, can be actuated either statically or cycled at a varying frequency to obtain a desired yawing moment. In order to obtain a wide and well-resolved spectrum of generated side forces, different configurations of DFEs were used. A specific configuration was defined and tested according to; (1) DFE location with respect to the

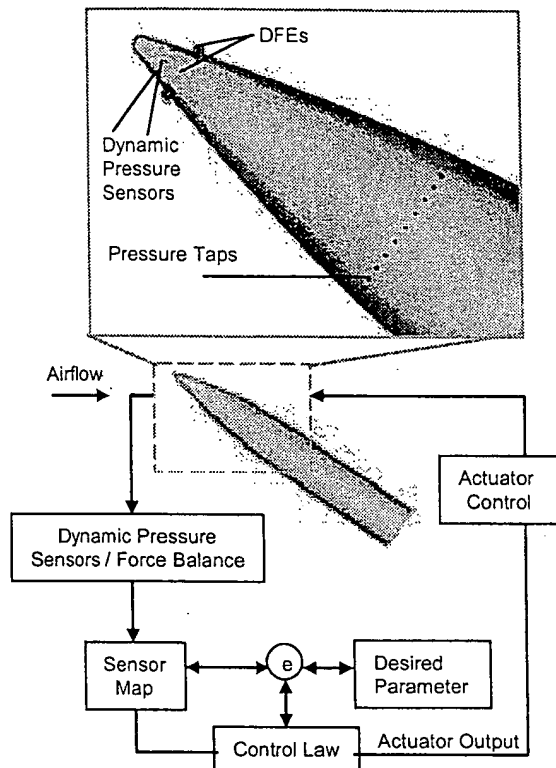


Figure 1. Schematic of the DFE-based phantom yaw control system.

flow, (2) number and pattern of DFEs, and (3) cycle frequency. Eight dynamic pressure sensors were flush-mounted circumferentially in front of the DFEs to capture instantaneous pressure fluctuations around the missile forebody. Data collected from the pressure sensors were correlated to the data obtained from the force balance to determine the optimal feedback parameter for the closed-loop controller. Figure 1 depicts the principle of operation of the DFE-based phantom yaw control system. The controller was designed to operate based on feedback information from either the pressure sensors or the force balance. In the presented work, the command input variable to the controller represented a specific desired flow state of the vortex system i.e., zero, left or right yaw. The controller determined the DFE actuation configuration in order to obtain the desired flow state based on an error, or the difference between the desired flow state and the actual flow state. Details on the feedback control system are presented in the later sections.

#### Missile Model

The model was a typical fin-less air-to-air missile with a fineness ratio of 6.12 based on the maximum body diameter and 3:1 tangent ogive nose, cone as shown in

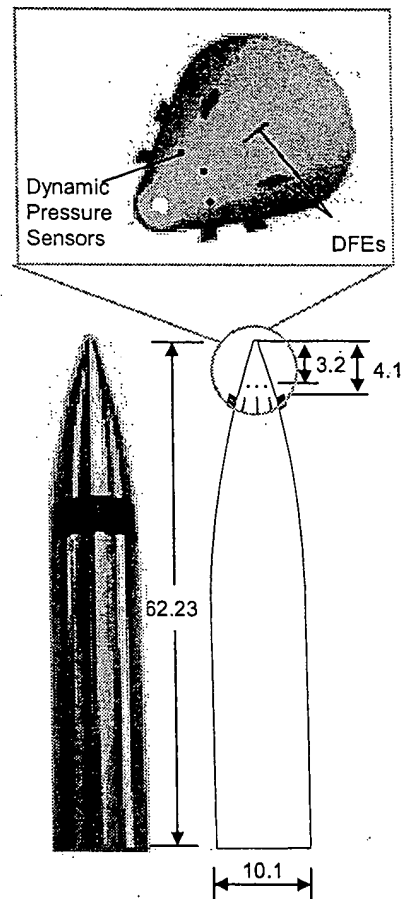


Figure 2. Illustration of the missile model with a 3:1 tangent ogive nose.

Figure 2. The length, maximum diameter, and the tip-radius of the missile model were 62.23 cm, 10.16 cm, and 0.635 cm respectively. The forebody contained circumferential arrays of eight DFEs and eight dynamic pressure sensors embedded near the tip, as shown in Figure 2. The dynamic pressure sensors used were EPE-83 series from Entran®.

In addition to the dynamic pressure sensors, the model was equipped with a total of 128 pressure taps (4 rings of 32 taps) to measure body pressure measurements (using a PSI™ Scanner Module). The forebody also contained a pneumatic Control Actuation System (CAS) shown in Figure 3 that enabled flush mounting as well as cycling of the DFEs. A housing (base) made of a light weight rigid material-Delrin, was designed and fabricated to fit readily inside the nose cone in order to hold the DFEs beneath the model surface. An elastomer was placed between the base plate and the plenum, covered by an O-ring to make the seal leak-proof. The base plate housed the DFEs in such a way that the elastomer

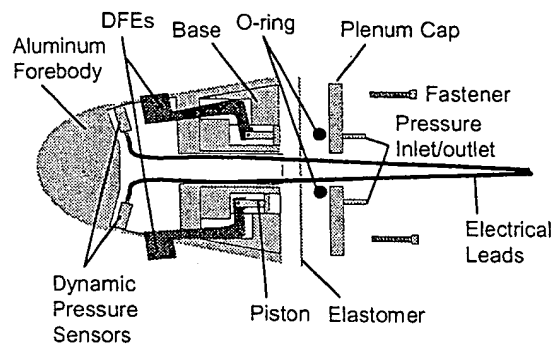


Figure 3. Illustration of the missile nose cone showing details of the DFE - Control Actuation System (CAS).

actuates the DFES pneumatically. On the whole, the CAS requires a high-pressure source, a valve, a plenum, an O-ring, power supply, and pneumatic lines. The units were installed internally in such a way that the DFES were flush to the model surface eliminating any obstruction into the flow. The model was equipped with a stinger-mounted force balance consisting of two strain gages to form a pitch and yaw moment measurement system. All data were collected on a personal computer based data acquisition system running LabVIEW™. Additional flow information was gathered using smoke and laser sheet flow visualization techniques. Information collected by the dynamic pressure sensors and the force balance was used to determine the configuration of DFES for the desired control effect at a given flight condition. Figure 4 shows the experimental set-up for wind tunnel testing.

#### Experimental Facility

Wind tunnel tests were performed at The University of Toledo, Fluids Dynamics Laboratory in a 3 x 3 ft. closed-loop low-speed wind tunnel. The model support incorporated a C-strut and a turntable to allow for different  $\alpha$ . A motor was incorporated in the turntable to facilitate remote model positioning and  $\alpha$ -sweep for testing. A dynamic turntable was also installed to facilitate dynamic tests on the model for sweep rates from 1 deg/s up to 120 deg/s (Aerotec ADR series direct-drive rotary stage table). The turntable had a direct-drive brushless servomotor, cog-free design, direct coupled, high-accuracy rotary encoder, and high-accuracy angular bearings. A 14-blade, variable-pitch fan coupled to a 150-hp electric motor was used to drive the flow. By varying the speed of the motor, the tunnel speed could reach over 200 mph (300 ft/s). Two tempered-glass sidewalls and a large Plexiglas window on the ceiling provided easy access for flow visualizations. The flow

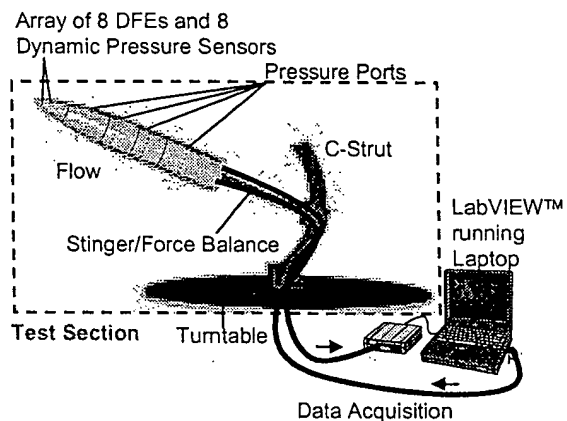


Figure 4. Experimental set-up for wind tunnel testing.

in the test-section was uniform, with a turbulence level of 0.2% outside of wall boundary layers.

#### Wind Tunnel Experiments

Open and closed-loop flow control experiments were conducted on the forebody model for  $\alpha$  ranging from 25° to 65° at a  $Re_d$  of  $0.13 \times 10^6$ . Open-loop experiments consisted of a series of static tests to characterize and optimize the effectiveness of DFES for the control of forebody flow asymmetry. Closed-loop experiments include dynamic tests to evaluate the performance of the control law in manipulating vortices for a desired yaw moment, as well as characterizing the effect of DFES during pitching maneuvers for different sweep rates. Details on the closed-loop control law for the high-alpha phantom yaw control system will be discussed in later sections. Data from dynamic pressure sensors, static pressure ports, force balance, and flow visualization were evaluated to determine, qualitatively and quantitatively, the effectiveness of the DFE-based phantom yaw control system.

#### Static Tests

Static wind tunnel tests were performed for  $\alpha$  ranging from 25° to 65° at a  $Re_d$  of  $0.13 \times 10^6$  based on the freestream velocity of 20 m/s and model diameter of 10.16 cm. Specific objectives of the static tests were to,

- (1) Determine the range of  $\alpha$  for which the DFES were most effective in creating high yaw moments,
- (2) Determine optimal DFE radial location on the missile nose cone for the highest impact on flowfield,



Pitch	Sideslip	Actuated DFE #							
$\alpha$ in deg	$\beta$ in deg								
20	0	0	1	2	3	4	5	6	7
25		0	1	2	3	4	5	6	7
30		0	1	2	3	4	5	6	7
35		0	1	2	3	4	5	6	7
40		0	1	2	3	4	5	6	7
45		0	1	2	3	4	5	6	7
50		0	1	2	3	4	5	6	7
55		0	1	2	3	4	5	6	7
60	▼	0	1	2	3	4	5	6	7

Table 1. Test matrix to determine the effective alpha range for the DFEs.

$\alpha = 40^\circ, \beta = 0^\circ$		$\alpha = 45^\circ, \beta = 0^\circ$		$\alpha = 50^\circ, \beta = 0^\circ$	
DFE#	$\theta$ in deg	DFE#	$\theta$ in deg	DFE#	$\theta$ in deg
1	0	1	0	1	0
1	5	1	5	1	5
1	10	1	10	1	10
1	15	1	15	1	15
1	20	1	20	1	20
1	22.5	1	22.5	1	22.5
1	25	1	25	1	25
1	30	1	30	1	30
1	35	1	35	1	35
1	40	1	40	1	40
2	22.5	2	22.5	2	22.5
3	22.5	3	22.5	3	22.5
4	22.5	4	22.5	4	22.5
5	22.5	5	22.5	5	22.5
6	22.5	6	22.5	6	22.5
7	22.5	7	22.5	7	22.5
0	22.5	0	22.5	0	22.5

Table 2. Test matrix to determine optimal DFEs radial location on the missile nose cone.

- (3) Characterize the effect of model imperfections on baseline asymmetry, and
- (4) Obtain a wide spectrum of generated control forces by optimally located DFEs at different alpha.

To obtain a range of alpha for which the DFEs were most effective, static tests were performed at varying pitch ( $\alpha$  ranging from  $20^\circ$  to  $65^\circ$  in steps of  $5^\circ$ ) for zero sideslip ( $\beta$ ) (see Table 1). During these tests, all the eight DFEs were deployed individually to determine the maximum generated force for each  $\alpha$ . Results from these tests revealed that the DFEs were most effective for

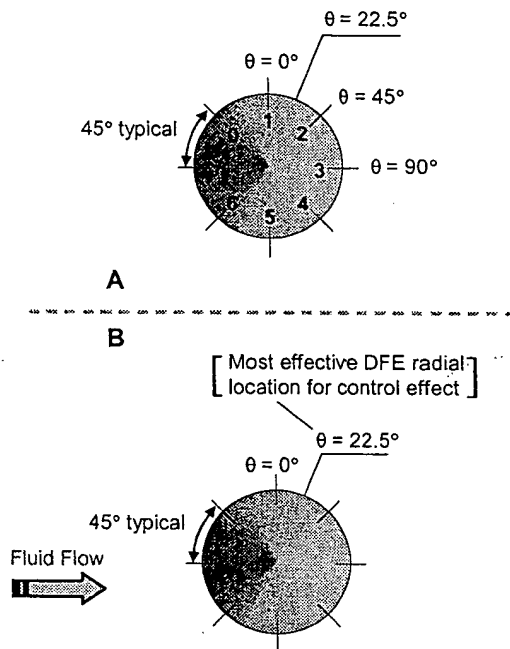


Figure 5. Illustrations of the missile nose showing DFE radial locations.

$40^\circ$ ,  $45^\circ$ , and  $50^\circ$   $\alpha$ . Additional static were conducted at these angles to determine optimal DFE radial location,  $\theta$ , on the missile nose cone, as seen in Table 2 ( $\theta$  is defined as the angle between the DFE position and the apex of the missile nose cone, as shown in Figure 5A). Tests shown in Table 2 were conducted to determine the DFE effectiveness in generating control forces for  $\theta$  ranging from  $0^\circ$  to  $40^\circ$  in steps of  $5^\circ$  rotated clockwise for  $0^\circ$   $\beta$  and  $40^\circ$ ,  $45^\circ$ , and  $50^\circ$   $\alpha$ . Additional fine-tuning tests revealed that the DFEs were most effective at  $22.5^\circ$   $\theta$  (see Figure 5B), which was also the best orientation for the natural flow asymmetry (near zero yaw).

Once optimal  $\theta$  ( $22.5^\circ$ ) for DFE actuation on the nose cone was determined, a series of tests were conducted with all the eight DFEs offset by  $22.5^\circ$  to, (1) find the best orientation for natural asymmetry, and (2) characterize the effect of model imperfections on baseline asymmetry. Additional tests listed in Table 3 were conducted with different DFE configurations at  $40^\circ$ ,  $45^\circ$ , and  $50^\circ$   $\alpha$  and  $0^\circ$   $\beta$  to provide a complete spectrum of possible control forces. DFE configurations consisted of static deployment of individual DFEs, cycling of one or more DFEs at varying frequencies, or combinations of both.

Configuration Table for Flow Effector(s) Deployment							
No.	DFE(s)	Static	Hz	No.	DFE(s)	Static	Hz
1	5	static	-	31	3 & 5	-	6 & 6
2	6	static	-	32	3 & 5	-	5 & 3
3	5	-	6	33	3 & 5	-	2 & 7
4	5	-	8	34	3 & 5	-	2 & 4
5	5	-	14	35	3 & 5	-	15 & 10
6	5	-	20	36	3 & 5	-	8 & 12
7	5	-	11	37	3 & 5	-	20 & 14
8	5	-	17	38	3 & 5	-	18 & 13
9	5	-	3	39	3 & 5	-	9 & 6
10	5	-	1	40	3 & 5	-	16 & 8
11	5	-	5	41	3 & 5	-	4 & 1
12	5	-	2	42	3 & 5	-	19 & 7
13	5	-	4	43	3 & 5	-	12 & 16
14	5	-	1	44	3 & 5	-	14 & 20
15	6	-	3	45	3 & 5	-	13 & 3
16	6	-	1	46	3 & 5	-	17 & 11
17	6	-	2	47	3 & 5	-	2 & 3
18	0	static	-	48	1	static	-
19	6 & 7	-	3 & 2	49	3	-	14
20	5 & 7	-	2 & 1	50	3	-	20
21	5 & 7	-	1 & 2	51	3	-	17
22	6	-	5	52	3	-	4
23	6	-	4	53	3	-	2
24	4	static	-	54	3	-	8
25	7	static	-	55	3	-	5
26	3 & 5	-	10 & 5	56	3	-	11
27	3 & 5	-	11 & 4	57	2	static	-
28	3 & 5	-	7 & 2	58	3	-	6
29	3 & 5	-	3 & 5	59	3	-	3
30	3 & 5	-	3 & 6	60	3	static	-

Table 3. DFE configuration test matrix to obtain a wide spectrum of generated forces for  $\alpha = 40^\circ$ ,  $45^\circ$ , and  $50^\circ$ .

#### Static Tests: Results and Discussion

Results are presented primarily in the form of control maps consisting of side force coefficients obtained via a series of DFE actuation cases listed in Tables 1-3. Preliminary tests identified the most effective  $\alpha$  range for the DFEs to be  $40^\circ$ ,  $45^\circ$ , and  $50^\circ$ . This is in agreement with the study conducted by Malcolm,<sup>31</sup> where strakes were found to be most effective for the similar  $\alpha$  range. Static deployment of DFEs at  $\alpha = 60^\circ$  produced large changes in effective moment on the slender body and demonstrated the

reversal of the asymmetric vortices. For  $40^\circ > \alpha > 60^\circ$ , no significant forebody asymmetric vortices were observed since the flow at such  $\alpha$  moves the separation region towards aftbody resembling wake flow phenomena; thus the effectiveness of the DFEs deteriorated since the control forces generated by the DFEs were not strong enough to counter act the phantom yaw created by flow separation. Laser sheet flow visualization (Figure 6) of the baseline case and the case with deployed flow effectors at  $60^\circ \alpha$  demonstrated vortex control using two different DFEs. Figure 6(a) shows model orientation for flow visualization. Figure 6(b), (c), and (d) shows the vortex formations for no flow effector deployed, DFE 1 deployed (located at  $0^\circ \theta$ ) and DFE 5 deployed ( $180^\circ \theta$ ), respectively. Vortex reversal is clearly demonstrated upon switching the deployment of DFE 1 and DFE 5.

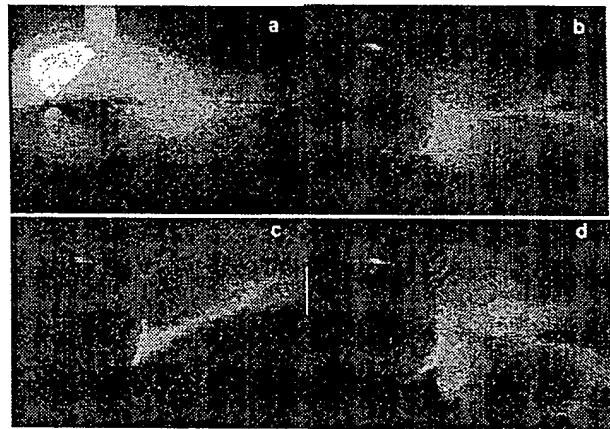


Figure 6. Laser sheet visualization of forebody vortex flows at  $60^\circ \alpha$ . (a) Missile model (b) Baseline vortex flow with no DFE (c) DFE deployed at  $0^\circ \theta$  (d) DFE deployed at  $180^\circ \theta$ .

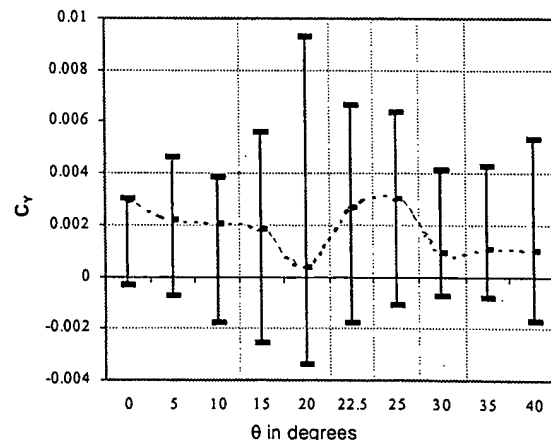


Figure 7. Control forces generated by DFE 1 at  $40^\circ \alpha$ ,  $0^\circ \beta$  and varying  $\theta$ .

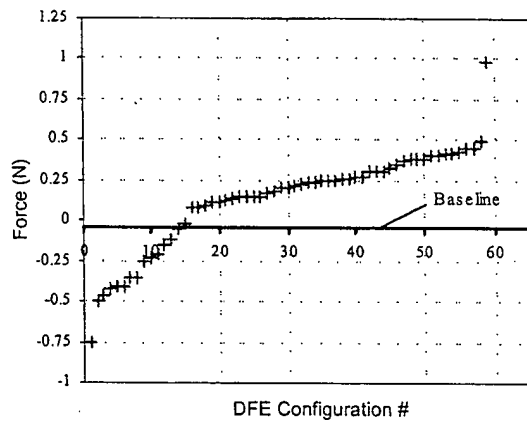


Figure 8. Spectrum of generated control forces using DFE configurations at  $40^\circ \alpha$  and  $0^\circ \beta$ .

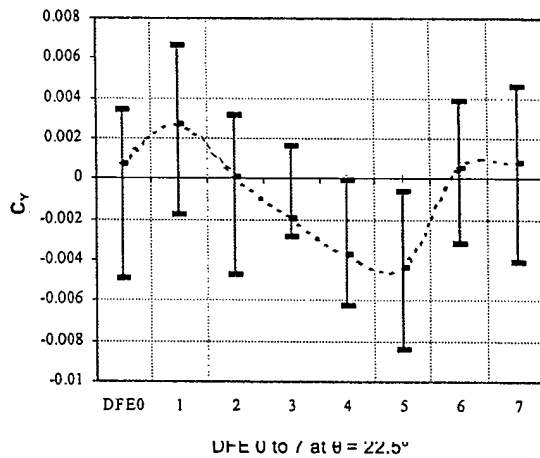


Figure 9. Control forces generated by DFEs 0 to 7 at  $40^\circ \alpha$ ,  $0^\circ \beta$  and  $22.5^\circ \theta$ .

Figure 7 shows the range of control forces at  $40^\circ \alpha$ ,  $0^\circ \beta$ , generated by DFE 1 for varying  $\theta$ . Variation of  $\theta$  was done by simply rotating the forebody in the clockwise direction. Significant controlled side forces were generated by DFE 1 when positioned between  $\theta = 15^\circ$  to  $25^\circ$ , as seen in Figure 7. The dashed-line cutting through all the vertical bars is the baseline force and the vertical bars represent a range of control forces that were generated by the DFE at the corresponding  $\theta$ . The range of forces was obtained by the configuration tests listed in Table 3. Each DFE was activated in turns and in combinations with other DFEs at varying frequencies. A typical plot showing the range of forces and the baseline is shown in Figure 8. While the largest control forces were generated from  $15^\circ$  to  $25^\circ \theta$ , the DFEs were still able to generate forces large enough to cancel the baseline asymmetry. In some conditions, DFEs were able to reverse the baseline flow asymmetry with an equal magnitude or higher. Figure 9 shows the range of forces

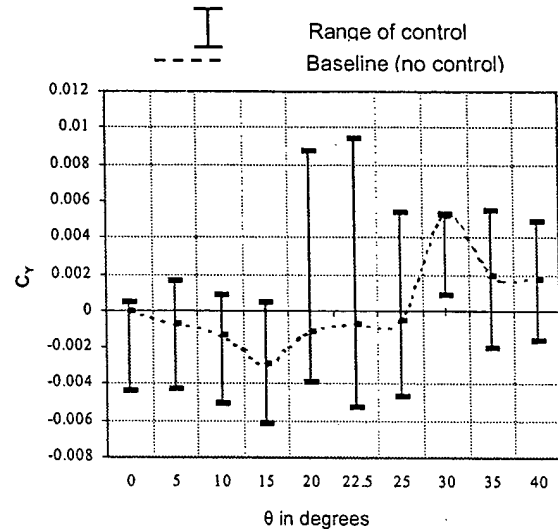


Figure 10. Control forces generated by DFE 1 at  $45^\circ \alpha$ ,  $0^\circ \beta$  and varying  $\theta$ .

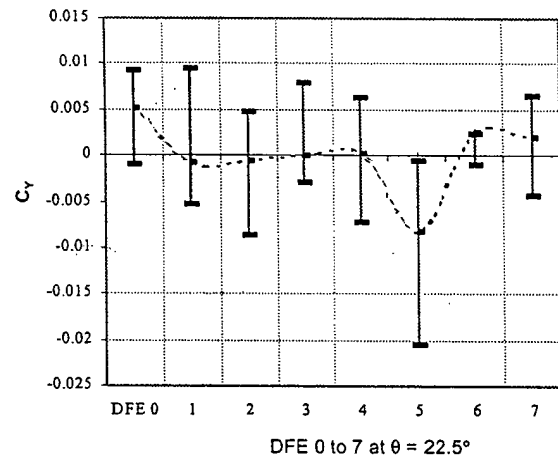


Figure 11. Control forces generated by DFEs 0 to 7 at  $45^\circ \alpha$ ,  $0^\circ \beta$  and  $22.5^\circ \theta$ .

generated by all the eight DFEs located at  $22.5^\circ \theta$  (deployed individually). These tests showed that even though the baseline flow asymmetry tends to behave in a disorderly fashion, the control forces generated by the DFEs were able to cancel and flip the vortices. Figures 10-13 shows similar control maps for  $45^\circ$  and  $50^\circ \alpha$  and  $0^\circ \beta$ .

### Closed-loop Control System

A closed-loop control system for high alpha forebody vortex control was developed using a digital Proportional Integral Derivative (PID) control law. The control law block diagram for the feedback controller used for the control of asymmetric vortices is shown in Figure 14. The command input variable,  $C_n$ , representative of a desired yawing moment (left, right, or zero) was compared to the existing flow

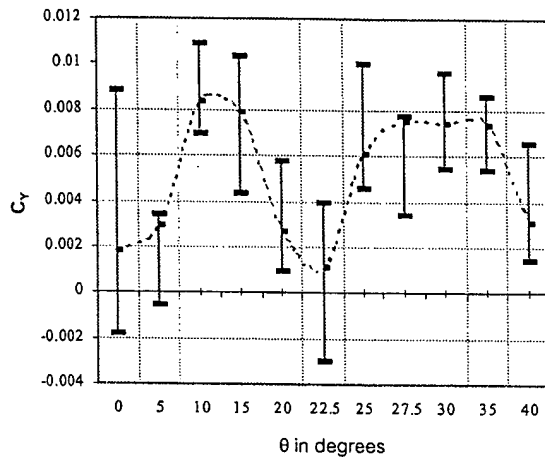


Figure 12. Control forces generated by DFE 1 at 50°  $\alpha$ , 0°  $\beta$  and varying  $\theta$ .

state  $C_n$  to obtain an error signal. The error value was used to determine DFE deployment state through mapping functions, which determined the proper actuator commands. The closed-loop control system focused specifically on determining the optimal timing for DFE deployment based on dynamic pressure signals in order to create a desired side force for the given flow conditions.

The primary goal of the previous experimental characterization of the forebody model was to gain insight into the flow physics of the asymmetry vortex control and manipulation along the slender body. Sensor information obtained from the dynamic pressure sensors located on the missile nose cone and the stinger mounted force balance was correlated to specific flow field event in order to develop an effective feedback control. As commonly found, the system dynamics were very

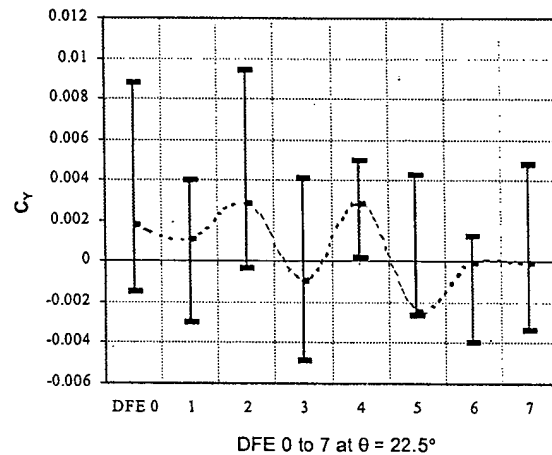


Figure 13. Control forces generated by DFEs 0 to 7 at 50°  $\alpha$ , 0°  $\beta$  and 22.5°  $\theta$ .

different from the uncontrolled system. An entire series of tests were conducted in a variety of flow conditions to provide experimental information to enable characterization of the influence of the DFEs on the flow field and the variables of interest (yawing moment and static pressure distribution). Similar to the original baseline flow evaluations; data were collected from a number of different conditions to develop a database of experimental knowledge of the system dynamics suitable for developing a real-time feedback controller. Using the empirical knowledge gained during the experimental testing, a frequency based control law was developed to actuate the active flow control devices based on either, localized pressure information or the force balance data.

The control program was written in LabVIEW™ and used a 12-bit National Instruments

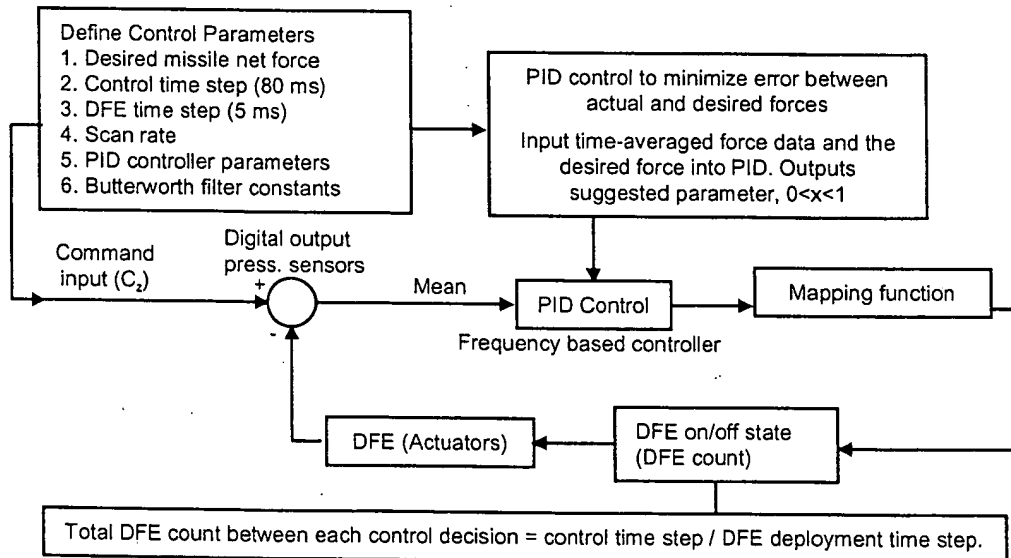


Figure 14. Block diagram of the closed-loop flow control system.

7344 Motion Board (PXI-7344). A National Instruments break-out box connected via USB to the Motion Control Board was used to route data from sensors and to deploy the DFEs. The frequency response of the actuator and the associated pneumatics defined the limits of the operating frequency. The DFEs were limited to approximately 100 Hz, or 10 ms for a complete DFE cycle (deploy and retract). Thus, to maximize DFE response time, a control input to deploy or retract was set to 5 ms (200Hz). The output from the control program was set for every 80 ms, or 13 Hz. Control inputs included eight embedded pressure sensors near the tip of the missile nose. The dynamic sensors, which provided the static pressure distribution around the nose cone were used to neutralize the missile's natural side force, as well as create an opposing side force. This was achieved by the controller that monitored the signals from two diametrically opposing pressure sensors. The sign of the pressure differential from these two sensors indicated the direction of the pressure gradient and thus the direction of the natural side force. In addition to the pressure sensors, the force balance was also used to provide magnitude and direction of the natural side force. The force balance was used in the final testing and demonstration of the control system since it provided the magnitude of the generated control forces. On the front panel of the control-demo program, the user specified the PID parameters (set values:  $K_p = 1.0$ ,  $K_i = 0.3$ ,  $K_d = 0.2$ ); filter coefficients, scan rate, control time step, DFE time step and the desired volts, which corresponded to a specific yawing moment coefficient  $C_n$ . The control output variable was also a value on voltage that corresponded to a specific value  $C_n$  value. The program consisted of a system to initialize hardware, compute a running average of force data, execute a PID sub-routine, and perform a mapping function for each DFE. Filtered running average force data was provided to PID controller input. The output of the PID was a value ( $x$ ) between 0 and 1 and was representative of the error between the actual and desired forces. This output at every 80 ms, was used in a mapping function to "map" the deployment sequence for the following 80 ms, in 5 ms intervals (the response time of the DFEs). Each DFE array was assigned a function  $f_n(x)$  that was used to determine the amount of time the DFEs were to be deployed over the period of 80 ms in order to achieve the desired side force. The PID output  $x$  was used to test the response of the system over the control time step.

The closed-loop control demonstration used two DFEs located at  $\theta = 22.5^\circ$  and  $157.5^\circ$  on the missile nose cone. Based on static wind tunnel tests, these DFEs were found to have the largest impact on the controllability of asymmetric vortices around the forebody and could thus generate the moment needed to eliminate the natural yawing moment on the missile. The mapping function

then addressed these two DFEs with instructions for a deployment sequence every 80 ms. The total PID range varied from  $-0.5$  to  $0.5$ . The mapping function for DFE 1 was  $f_1(x) = 1 - (x + 0.5)$  and for DFE 2 was  $f_2(x) = x + 0.5$ . These functions could easily be applied to arrays of DFEs to fine-tune the closed-loop control. After the deployment count was completed, the DFEs were instructed to remain retracted for the remainder of the 16 counts. This closed-loop control program successfully mitigated side forces responsible for phantom yaw, enhanced the side force in the same direction of the naturally occurring phantom yaw, and produced side forces in the opposite direction of phantom yaw.

### Dynamic Tests

Dynamic tests were performed to demonstrate the ability of the feedback controller in stabilizing and controlling forebody flow asymmetries at high alpha. Dynamic experiments were conducted using the stinger mount force balance, DFEs, and a PID closed-loop controller. Dynamic pitching tests were conducted on a high-speed turntable with pitching rates up to  $120^\circ/\text{s}$ . The turntable was controlled via a computer using a LabVIEW<sup>TM</sup> program interface that collected the force balance strain gage voltage. The voltage reading corresponded a specific yawing force produced from the natural asymmetric vortex shedding, as well as the DFE-generated yaw force. Three separate dynamic tests were conducted; 1) dynamic pitching tests without the controller, 2) controller modulated yaw forces, and 3) closed-loop control dynamic sweeps. The objective of these tests were to, (1) characterize the effects of dynamic sweep from  $0^\circ - 60^\circ \alpha$  on the asymmetric vortices formed on the missile forebody, (2) characterize the effects of DFEs in controlling the asymmetric vortex shedding, (3) modulate yawing moments using optimized DFE configuration at high alpha ( $60^\circ \alpha$ ), and (4) control the missile model during a dynamic sweep from  $0^\circ - 60^\circ \alpha$  using the feedback controller.

#### Test 1: Dynamic pitching

Dynamic pitching tests from  $0-60^\circ \alpha$ ,  $0^\circ \beta$  with sweep rates ranging of  $1^\circ/\text{s}$  up to  $120^\circ/\text{s}$  were performed at a dynamic pressure of  $5 Q$  and a  $Re_d$  of 0.13 million. Characterization of the missile model and the DFE-effects during dynamic pitching was obtained from these tests.

#### Test 2: Controller Modulated Yaw Forces

Controller modulated tests consisted of the complete closed-loop yaw control system with the stinger mounted force balance, DFEs and the

controller. During these tests the model was held at  $60^\circ \alpha$  and  $0^\circ \beta$ . The user specified the desired force balance raw voltage (which corresponded to a specific yaw force in the flow state) for the model to achieve, and the controller triggered the specific DFE configuration to achieve the force. The control parameters for the controller to obtain the desired force were the DFE configuration and the duty cycle of DFEs located at  $\theta = 22.5^\circ$  and  $157.5^\circ$ . The controller's ability to manipulate the forebody flow asymmetries to obtain the desired yaw forces was successfully demonstrated during these tests.

### Test 3: Closed-Loop Control Dynamic Sweeps

This test was the demonstration of the closed-loop control system to maintain a zero yaw force during the dynamic pitching from  $0$ - $60^\circ \alpha$  at  $0^\circ \beta$ .

### Dynamic Tests: Results and Discussion

During the dynamic pitching characterization tests it was observed that large side forces occurs between  $40^\circ$  and  $60^\circ \alpha$ . For  $\alpha > 60^\circ$ , the effects of vortex shedding from the forebody decreased significantly due to diminishing influence of the axial flow component, resulting in reduced phantom yaw effect and more blunt body vortex shedding. It was observed that as the pitching rates increased, there was a time delay in the formation of forebody asymmetric vortex shedding due to the difference in time scales of the pitch-up maneuver and the formation of vortices, resulting in low side forces at  $\alpha$  for which large side forces were noticed during low pitching rates. The time lag for the formation of asymmetric vortex shedding became so large at pitching rate of  $120^\circ/\text{s}$ , that the side forces produced due to asymmetric forebody shedding did not occur until the model was held at a fixed  $60^\circ \alpha$  after the pitching motion was completed.

Figure 15 shows yawing moment coefficient variation with  $\alpha$  and time during pitch-up maneuver at  $10^\circ/\text{s}$  for uncontrolled (baseline) and DFE-actuated cases. The baseline flow asymmetry changes significantly between  $45^\circ$  and  $60^\circ \alpha$ . The DFEs located at the optimal positions,  $22.5^\circ \theta$  and  $67.5^\circ \theta$ , were deployed in separate pitch-up tests to capture the effects of the devices on flow asymmetry. The baseline (no DFE) had a flow asymmetry yielding a positive yawing moment between  $45^\circ$  and  $60^\circ \alpha$ . The DFE at  $22.5^\circ \theta$  strengthened the flow asymmetry in the same direction while the DFE located at  $67.5^\circ \theta$  forced the vortex reversal to create the opposite yawing moment between  $45^\circ$  and  $60^\circ \alpha$ . Similar characteristic curves for pitching rate of  $35^\circ/\text{s}$  is shown in Figure 16 (pitch-up) and Figure 17 (pitch-down). Comparison of Figures 16 and 17 demonstrate similar effects of the DFEs and baseline on forebody flow asymmetries. During pitch-down

maneuver, DFE located at  $22.5^\circ \theta$  starts off at a large yawing moment value at  $60^\circ \alpha$  and drops to the moment values similar to those obtained during pitch-up and baseline for  $\alpha$  between  $0^\circ$  and  $40^\circ \alpha$ .

The force modulation tests at  $60^\circ \alpha$  were successful in demonstrating the ability of the control system to generate control forces in both, positive and negative yaw direction, using two DFEs located at  $\theta = 22.5^\circ$  and  $157.5^\circ$  integrated with the closed-loop controller. Figure 18 shows that the controller was able to actuate the DFEs to precisely generate a desired positive and negative side force to follow the yaw commanded by the user. The plot shows the commanded yaw versus the yaw generated by the DFEs using the closed-loop control system. The user commanded yaw values ranged from  $100\%$  to  $33\%$  of the maximum achievable yaw by the DFEs at  $60^\circ \alpha$  in both positive and negative direction. The user entered a desired volt-value which corresponded to a particular yaw-force and the controller calculated the current yaw-force to obtain an error signal for the controller to determine the DFE actuator configuration, i.e. DFE#, frequency, and time of deployment, in order to obtain the desired yaw-force. Fig. 18 shows that the control system was successfully able to generate the desired yaw value.

Figure 19 shows the control map obtained from different closed-loop experiments to demonstrate the ability of the controller to generate the desired yaw moments during pitching maneuvers from  $0^\circ$  -  $60^\circ \alpha$ . The baseline characterization showed a positive natural asymmetry above  $40^\circ \alpha$ . During the first test, the DFEs were deployed to control the baseline force to a fixed yaw value, the second test demonstrated the ability of the DFE to generate a positive yawing moment and the third test demonstrated the ability to flip the positive yawing moment into a negative yawing moment. The superposition plot of these three tests (Figure 19) clearly shows the effectiveness of the presented DFEs-based closed-loop system to provide phantom yaw control of missiles during such a dynamic pitching maneuver.

### Conclusions

An experimental study to demonstrate a high alpha phantom yaw control system for enhanced missile maneuverability and stabilization was conducted. It was found that the DFE configuration parameters; position and frequency of operation, were critical to obtain the desired force during both, static and dynamic tests. Results demonstrated the ability of the control system to generate a desired side force corresponding to zero, left and right yaw using the DFEs integrated with the closed-loop controller.

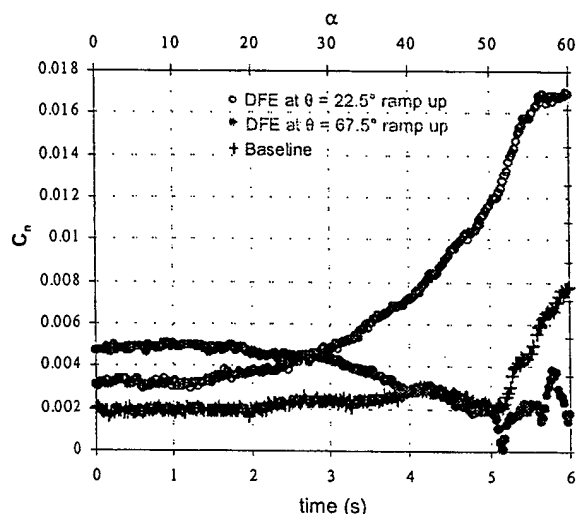


Figure 15. Characteristic curves: baseline and DFE-actuation for pitch-up maneuver at 10°/s.

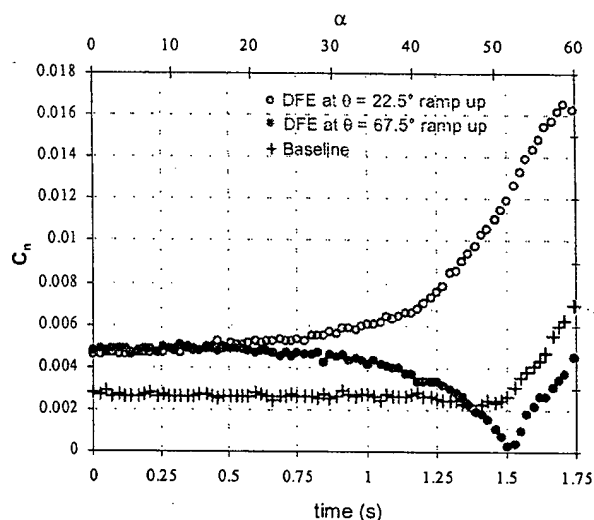


Figure 16. Characteristic curves: baseline and DFE-actuation for pitch-up maneuver at 35°/s.

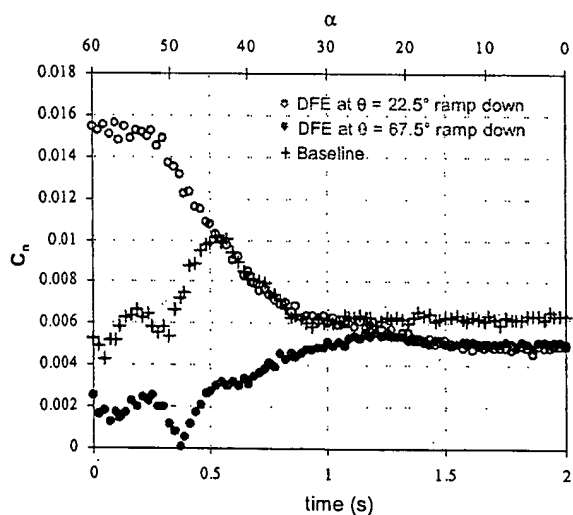


Figure 17. Characteristic curves: baseline and DFE-actuation for pitch-down maneuver at 35°/s.

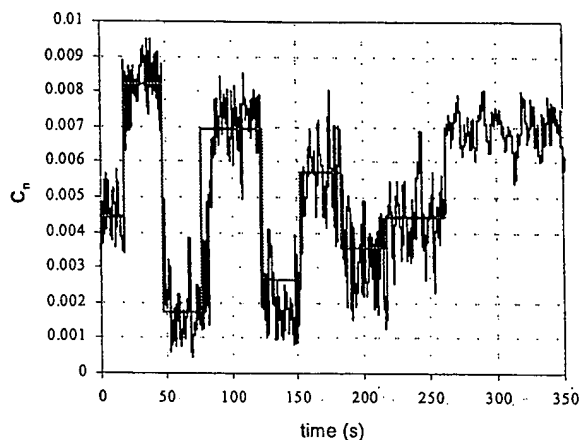


Figure 18. User specified yawing moment modulation at 60°  $\alpha$  using DFEs and the closed-loop feedback controller.

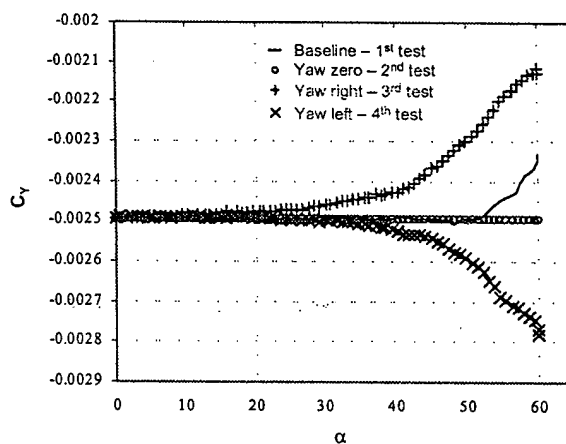


Figure 19. Control authority chart of the high alpha phantom yaw control system showing baseline, zero, left, and right yaw forces generated using DFEs.

### Acknowledgements

This investigation was conducted with support from the Air Force Research Lab under a Phase II SBIR award. Special thanks go to Dr. Carl Tilmann of AFRL for his interest and providing impetus to this research.

### References

- <sup>1</sup>Herbst, W. B., "Supermaneuverability," *Proceedings of the Workshop on Unsteady Separated Flow*, edited by M. S. Francis and M. W. Luttges, U.S. Air Force Academy, 1983, pp. 1-9.
- <sup>2</sup>Herbst, W. B., "Future Fighter Technologies," *Journal of Aircraft*, Vol. 17, No. 8, 1980, pp. 561-566.

<sup>3</sup>Ashley, H., "On the feasibility of Low-Speed Aircraft Maneuvers Involving Extreme Angles of Attack," *Journal of Fluids and Structures*, Vol. 1, July 1987, pp. 319-335.

<sup>4</sup>Gapcynski, J. P., "An Experimental Investigation of the Flow Phenomena over Bodies at High Angles of Attack at a Mach number of 2.0," NACA RM-L55H29, Oct. 1955.

<sup>5</sup>Gowen, F. E., and Perkins, E. W., "A study of the Effect of Body Shape of the Vortex Wakes of Inclined Bodies at a Mach Number of 2," NACA RM-A53117, Dec. 1958.

<sup>6</sup>Ericsson, L. E., and Reding, J. P., "Asymmetric Flow Separation and Vortex Shedding on Bodies of Revolution," *Tactical Missile Aerodynamics*, edited by M. J. Hemsch, Vol. 141, Progress in Aerospace and Aeronautics, AIAA, New York, 1991, pp.391-452.

<sup>7</sup>Thomson, K. D., and Morrison, D. F., "On the Asymmetric Vortex Shedding from Slender Cylindrical Bodies at Large Angles of Yaw," Weapon Research Establishment, Australia, TN-HSA 106, May 1965.

<sup>8</sup>Ericsson, L. E., "Unsteady Flow Separation on Slender Bodies at High Angles of Attack," AIAA Paper 90-2835, Jan. 1990.

<sup>9</sup>Pick, G. S., "Investigation of Side Forces on Ogive-Cylinder Bodies at High Angles of Attack in the  $M = 0.5$  to 1.1 Range," AIAA Paper 71-570, June 1971.

<sup>10</sup>Wardlaw, A. B., Jr., "High Angle of Attack Missile Aerodynamics," Paper 5, AGARD LS-98, March 1978.

<sup>11</sup>Jorgenson, L. H., "Prediction of Aerodynamic Characteristics of Slender Bodies Alone and With Lifting Surfaces to High Angles of Attack," Paper 28, AGARD-CP-247, Oct. 1978.

<sup>12</sup>Chapman, G. T., and Keener, E. R., "The Aerodynamics of Bodies of Revolution at Angles of Attack to  $90^\circ$ ," AIAA Paper 79-0023, Jan. 1979.

<sup>13</sup>Ericsson, L. E., and Reding, J. P., "Review of Vortex-Induced Asymmetric Loads - Part I," *Zeitschrift fuer Flugwissenschaften und Weltraumforschung*, Vol. 5, No. 3, 1981, pp. 162-174.

<sup>14</sup>Ericsson, L. E., and Reding, J. P., "Review of Vortex-Induced Asymmetric Loads - Part II," *Zeitschrift fuer Flugwissenschaften und Weltraumforschung*, Vol. 5, No. 6, 1981, pp. 349-366.

<sup>15</sup>Ericsson, L. E., and Beyers, M. E., "Conceptual Fluid/Motion Coupling in the Herbst Supermaneuver," *Journal of Aircraft*, Vol. 34, No. 3, 1997, pp. 271-277.

<sup>16</sup>Rao, D. M., "Side Force Alleviation on Slender, Pointed Forebodies at High Angles of Attack," *Journal of Aircraft*, Vol. 16, No. 11, pp.763-768, 1979.

<sup>17</sup>Modi, V. J., and Stewart, A. C., "Approach to Side Force Alleviation Through Modification of the Pointed Forebody Geometry," AIAA Paper 90-2834, Jan. 1990.

<sup>18</sup>Fisher, D. F., and Cobleigh, B. R., "Controlling Forebody Asymmetries in Flight-Experience with Boundary Layer Transition Strips," NASA Technical Memorandum 4595, 1994.

<sup>19</sup>Ericsson, L. E., "Unsteady Flow Separation on Slender Bodies at High Angles of Attack," AIAA Paper 90-2835, Jan. 1990.

<sup>20</sup>Maynes, R. D., and Gebert G. A., "Rotating Nose Tip Effects on Slender Body Aerodynamics at High Angles of Attack," *Journal of Spacecraft and Rockets*, Vol. 32, No. 6, 1995, pp. 944-950.

<sup>21</sup>Stahl, W., "Suppression of Asymmetry of the Vortex Flow Behind a Circular Cone at High Incidence," AIAA Paper 89-3372-CP, Aug. 1989.

<sup>22</sup>Ng, T. T., "Effect of a Single Strake on the Forebody Vortex Asymmetry," *Journal of Aircraft*, Vol. 27, No. 9, 1990, pp.161-184.

<sup>23</sup>Sharic, D., Portnoy, H., and Rom, J., "A Study of the Effects of Jets Injected from a Slender Body of Revolution on the Side Forces Acting on it at Large Angles of Attack in Low Speeds," Technion - Israel Inst. of Technology, Dept. of Aeronautical Engineering, TAE 337, 1978.

<sup>24</sup>Roos, F. W., "Microblowing for High-Angle-of-Attack Flow Control on a Fighter Aircraft," AIAA Paper 96-0543, January 1996.

<sup>25</sup>Malcolm, G. N., and Ng, T. T., "Aerodynamic Control of Fighter Aircraft by Manipulation of Forebody Vortices," CP-497, AGARD Paper 15, Nov. 1991.

<sup>26</sup>Williams, D., and Bernhardt, J., "Proportional Control of Asymmetric Forebody Vortices with the Unsteady Bleed Technique," AIAA Paper 90-1629, June 1990.

<sup>27</sup>Bernhardt, J., and Williams, D., "Effect of Reynolds Number on Control of Forebody Asymmetry by Suction and Bleed," AIAA Paper 93-3265, July 1993.

<sup>28</sup>Patel, M. P., Ng, T. T., Lisy, F. J., Prince, T. S., and DiCocco, J. M., "MEMS Deployable Flow Effectors for Missile Control," *Proceedings of the 20<sup>th</sup> AIAA Missile Sciences Conference*, California, 2000.

<sup>29</sup>Buffington, J. M., and Adams, R. J., "Nonlinear Vortex Flow Control for High Angle of Attack Maneuvering," *Control Engineering Practice*, Vol. 3, No. 5, 1995, pp. 631-642.

<sup>30</sup>Bernhardt, J. E., and Williams, D. R., "Closed-Loop Control of Forebody Flow Asymmetry," *Journal of Aircraft*, Vol. 37, No. 3, 2000, pp. 491-498.

<sup>31</sup>Malcolm, G. N., "Forebody Vortex Control - A Progress Review," AIAA Paper 93-3540, Aug. 1993.



**This Page is Inserted by IFW Indexing and Scanning  
Operations and is not part of the Official Record**

**BEST AVAILABLE IMAGES**

Defective images within this document are accurate representations of the original documents submitted by the applicant.

Defects in the images include but are not limited to the items checked:

- ☐ **BLACK BORDERS**
- ☐ **IMAGE CUT OFF AT TOP, BOTTOM OR SIDES**
- ☐ **FADED TEXT OR DRAWING**
- ☐ **BLURRED OR ILLEGIBLE TEXT OR DRAWING**
- ☐ **SKewed/SLANTED IMAGES**
- ☒ **COLOR OR BLACK AND WHITE PHOTOGRAPHS**
- ☒ **GRAY SCALE DOCUMENTS**
- ☒ **LINES OR MARKS ON ORIGINAL DOCUMENT**
- ☐ **REFERENCE(S) OR EXHIBIT(S) SUBMITTED ARE POOR QUALITY**
- ☐ **OTHER:** \_\_\_\_\_

**IMAGES ARE BEST AVAILABLE COPY.**

**As rescanning these documents will not correct the image problems checked, please do not report these problems to the IFW Image Problem Mailbox.**